Chlorine enhances nocturnal heterogeneous uptake of NO_2 in coastal atmosphere under sea-land breeze circulation

Ziyi Lin[1,2,3], Xiuwen Yong[1,2,4], Lingjun Li[1,2,3], Yuping Chen[1,2,3], Lingling Xu[1,2,3]*, Xiaoting Ji[1,2,3], Chen Yang[1,2,3], Keran Zhang[1,2,3], Feng Zhang,[1,2] Ziying Chen[1,2,3], Gaojie Chen[1,2,3], Xiaolong Fan[1,2], Mengren Li[1,2], Jinsheng Chen[1,2,3]*

Affiliations:

[1]State Key Laboratory of Advanced Environmental Technology, Institute of Urban Environment, Chinese Academy of Sciences, Xiamen 361021, China

[2]Fujian Key Laboratory of Atmospheric Ozone Pollution Prevention, Institute of Urban Environment, Chinese Academy of Sciences, Xiamen 361021, China

[3]University of Chinese Academy of Sciences, Beijing 100049, China

[4]Fujian Agriculture and Forestry University, Fuzhou, 350002, China

*Correspondence to: jschen@iue.ac.cn (Jinsheng Chen); Linglingxu@iue.ac.cn (Lingling Xu)

Abstract: Heterogeneous uptake of NO_2 serves as a significant source for reactive nitrogen species, playing an important role in atmospheric chemistry. Laboratory studies have demonstrated that chlorine can promote the heterogeneous NO_2 uptake, yet this effect under real ambient conditions remains poorly elucidated. Based on comprehensive field observations, a machine learning technique, and a multiphase chemical box model in the coastal city of Xiamen, China, this study reveals the enhancement effect of chlorine (Cl) on NO_2 uptake and quantifies the impact of this enhanced uptake on reactive nitrogen species during nocturnal sea-land breeze (SLB) periods. Compared with non-SLB days, nocturnal concentrations of nitrous acid (HONO) and particulate nitrate (NO_3^-) increased significantly during SLB days, with high mean value of NO_2 uptake rate constant (kNO_2) reaching 9.70×10^{-6} s^{-1}. Machine learning revealed that chlorine was the most important influencing factor for the enhanced kNO_2. Incorporating this kNO_2 into the chemical box model substantially resolved the underestimation of HONO concentration and NO_3^- production under SLB conditions. Notably, nocturnal NO_2 uptake dominated HONO formation (83.9%), while making a substantial contribution (46.4%) to nitrate formation. This study highlights the critical role of chlorine-enhanced NO_2 uptake in atmospheric reactive nitrogen cycling and provides valuable insights for nocturnal chemistry in complex coastal environments.

1. Introduction

Nitrous acid (HONO) and nitrate (NO_3^-) are key reactive nitrogen species in the atmosphere. HONO, a major source of OH radicals, significantly contributes to the formation of O_3 and secondary aerosols by influencing radical budget (Acker et al., 2006; Alicke et al., 2003). NO_3^- is an important chemical component of particulate matter (PM), contributing to PM pollution and acid rain (Cao et al., 2022; Qu and Han, 2021). As a crucial source of both HONO and NO_3^-, the heterogeneous uptake of NO_2 has attracted considerable attention (Xuan et al., 2025; Carter et al., 1982).

Traditionally, the uptake of NO_2 in bulk solution was considered extremely slow, and thus this process was often negligible (Lee and Schwartz, 1981). However, numerous field observations have indicated that NO_2 uptake plays a significant role in the formation of HONO and NO_3^-. Previous studies have revealed a strong correlation between NO_2 and HONO after excluding homogeneous formation and primary emissions, suggesting efficient heterogeneous conversion of NO_2 to HONO

(Su et al., 2008; Zhang et al., 2024). Studies have also found that incorporating NO_2 uptake mechanisms into models can substantially improve the HONO simulation, especially at night (Zhang et al., 2023; Xuan et al., 2024; Zhang et al., 2024; Shi et al., 2020). Using an aerosol-fog sampling system and a box model, Xu et al (Xu et al., 2024), found that NO_2 uptake was the primary driver of the rapid increase in NO_3^- during fog events. Currently, the reported reaction rate constant for NO_2 uptake vary widely across different types of surfaces, spanning several orders of magnitude from 10^{-7} s^{-1} to 10^{-5} s^{-1} (Zhang et al., 2025b). Multiple factors have been demonstrated to affect the NO_2 uptake rate constant (kNO_2) in laboratories, including NO_2 concentrations, aerosol particle size, ionic strength, pH, NH_3, and liquid water content (Liu and Abbatt, 2021; Gen et al., 2024; Zhang et al., 2025a). In the real atmosphere, research during haze events showed that parameterization schemes of kNO_2 considering relative humidity (RH) and NH_3 influences significantly improved the simulation results of heterogeneous HONO formation (Zhang et al., 2023). Long-term observations revealed that changes in aerosol chemical composition could alter aerosol pH, consequently affecting the uptake kinetics of NO_2 to HONO (Zhang et al., 2025b).

Investigations in coastal areas reported higher NO_2 uptake rates in marine air masses compared to continental ones (Zha et al., 2014; Yang et al., 2021), overall surpassing those measured at continental urban, suburban, and rural sites (Wentzell et al., 2010; Kleffmann et al., 2003; Zhang et al., 2020; Hao et al., 2020; Cui et al., 2018). These findings suggest that heterogeneous NO_2 uptake plays a particularly critical role in the coastal troposphere. Within the marine boundary layer, chloride ions are abundant due to sea spray. Chloride ions exhibit special surface propensity, making them tend to distribute at the air-water interface (Knipping et al., 2000; Piatkowski et al., 2014; Jungwirth and Tobias, 2006). Laboratory studies demonstrated that chloride ions can establish a surface-directed electric field, which attracts atmospheric NO_2 molecules and promotes their further uptake at air-water interface (Wang et al., 2025a; Zhang et al., 2025a). Nevertheless, the influence of chlorine on NO_2 uptake in realistic coastal atmosphere and the consequent impacts on reactive nitrogen cycling remain to be fully elucidated.

Sea-land breeze (SLB) events occur frequently in coastal urban areas (Chen et al., 2023; Liu et al., 2025; Xie et al., 2023). During SLB periods, the coastal boundary layer experiences intensive interactions between marine and continental air masses, providing a natural laboratory to investigate the effect of sea-salt chloride on NO_2 uptake. In this study, a multi-parameter field observation was conducted in Xiamen, a typical coastal city in China, during the autumn and winter seasons characterized by frequent SLB events (Chen et al., 2023). Based on observations, the characteristics of SLB days were revealed and kNO_2 under both SLB and non-SLB conditions were quantified. Using machine learning method, the significant promoting effect of chlorine on NO_2 uptake during nocturnal SLB periods was demonstrated. Furthermore, the obtained kNO_2 was incorporated into an advanced multiphase box model to evaluate the impact of chlorine-enhanced NO_2 uptake on atmospheric reactive nitrogen cycling. This study highlights the role of previously overlooked chlorine on NO_2 uptake for nocturnal chemistry in coastal atmosphere.

2. Methods

2.1 Field measurements and sea-land breeze identification

Our observations were conducted at the Atmospheric Observation Supersite (24.61°N, 118.06°E) of the Institute of Urban Environment (IUE), Chinese Academy of Sciences in Xiamen, from November 18, 2023 to January 6, 2024. Xiamen is a coastal city in southeastern China. The

observation site is located approximately 5 km from the shore and is surrounded by residential, commercial areas and major traffic arteries. Instruments were deployed on the roof of the IUE building at approximately 70 m above ground level. Virtually no high buildings obstructed the path between the site and the coast, making it a typical coastal urban site.

A suite of atmospheric parameters was observed simultaneously. Ambient HONO was measured online by a water-based long-path absorption photometer (Zhichen Beijing, China) (Xuan et al., 2024). Sulfuric acid (H_2SO_4) and HCl were measured using a long time-of-flight chemical ionization mass spectrometer, equipped with a nitrate reagent ion source (Aerodyne Research Inc., USA) (Yang et al., 2023). The chemical composition of $PM_{2.5}$ was analyzed using both a MARGA ADI 2080 (Metrohm Applikon, Switzerland) and an ACSM (Aerodyne Research Inc., USA) (Liu et al., 2022; Chen et al., 2022). Particle number size distribution (PNSD) in the range of 2–300 nm was measured by two scanning mobility particle sizers (TSI inc., USA) equipped with a long-DMA (2.5–62 nm) and a nano-DMA (7–300 nm), respectively (Li et al., 2025). Additionally, a range of commercial instruments were employed to monitor trace gases (NO, NO_2, SO_2, O_3, and VOCs), meteorological parameters (ambient temperature, RH, wind-speed, wind-direction and ultraviolet radiation), and photolysis rates (JO^1D, JNO_2, $JHONO$, JNO_3, $JHCHO$ and JH_2O_2) (Liu et al., 2022). Detailed descriptions of instrument operation, species identification, and calibration are provided in **Text S1**. Hourly BLH data were obtained from the ERA5 reanalysis dataset (Hersbach et al., 2020).

Sea-land breeze days were identified based on observed wind-speed and wind-direction according to the criteria established in our previous work (Chen et al., 2023). Briefly, the coastline in Xiamen is characterized by a northeast-southwest trend, the sea breeze is blowing from the east-south, and the land breeze is blowing from the west-north-northeast. According to observed wind direction, a natural day could be divided into four periods. Specifically, 01:00-08:00 LT (land breeze period), 13:00-20:00 LT (sea breeze period), and 09:00-12:00 LT and 21:00-24:00 LT (mixed sea-land breeze period). A day was classified as an SLB day if the following three conditions were met: (1) the 24-hour mean wind speed was < 10 m/s; (2) during the land breeze period, the land breeze persisted for ≥ 4 hours and the sea breeze lasted ≤ 2 hours; and (3) during the sea breeze period, sea breeze persisted for ≥ 4 hours and the land breeze lasted ≤ 2 hours. As shown in **Fig. S1** (light blue areas), a total of 23 SLB days were identified during the observation period. The remaining days were classified as non-SLB days. **Fig. S2** illustrates that the wind patterns on SLB days differed from those on non-SLB days, characterized by a higher prevalence of southeasterly sea breezes.

2.2 Calculation of HONO from heterogeneous formation processes and NO_2 uptake rate

Due to the absence of agricultural fields near the sampling site and its proximity to major traffic arteries, the primary emission of HONO was attributed to vehicles. Only nighttime data were used in our study, the uncertainties associated with photochemical process, such as NO_3^- photolysis were excluded. Therefore, the nighttime corrected HONO ($HONO_{corr}$) is calculated as follows:

$$HONO_{corr,t} = HONO_t - E_{vehicle,t} - P_{NO+OH,t} \quad (1)$$

where $HONO_t$ is the observed HONO concentration, $E_{vehicle,t}$ is the HONO emission from vehicles, and $P_{NO+OH,t}$ is the HONO production from homogeneous reactions. $E_{vehicle,t}$ is calculated as the NOx concentration multiplied by the emission factor 0.005 (Zhang et al., 2025b). $P_{NO+OH,t}$ is calculated as follows:

$$P_{NO+OH,t} = k_{NO+OH} \times [NO] \times [OH] \times 3600 \quad (2)$$

where k_{NO+OH} (cm^3 $molecules^{-1}$ s^{-1}) is calculated in the Master Chemical Mechanism 3.3.1 (MCM

v3.3.1 https://mcm.york.ac.uk/MCM/), 3600 s represents the 1 hour integration interval, and the concentration of OH radicals is estimated based on the steady-state balance of H_2SO_4 (Nie et al., 2022). Because H_2SO_4 is primarily produced by the reaction of SO_2 and OH and is mainly lost via condensation sink (CS) onto particle surfaces, the OH concentration can be estimated as below:

$$[OH] = \frac{[H_2SO_4]\times CS}{k_{OH+SO2}\times[SO_2]} \quad (3)$$

where k_{OH+SO2} is 5×10^{-13} cm^3/s (Seinfeld et al., 1998), and CS (/s) is calculated as follows (Kulmala et al., 2012):

$$CS = 2\pi D_v \int_0^{d_{p,max}} d_p\, \beta n(d_p) dd_p \quad (4)$$

where D_v is the diffusion coefficient of H_2SO_4, d_p is the particle diameter derived from the measured PNSD, β is the transitional correction factor, and $n(d_p)$ is the particle number concentration of diameter d_p.

In line with previous studies (Zhang et al., 2025b; Zhang et al., 2020; Zhang et al., 2024), the heterogeneous conversion of NO_2 to form $HONO_{corr}$ at night is considered a pseudo-first-order reaction. The reaction rate constant (k_{NO2}, s^{-1}) is calculated based on the conversion of NO_2 during a given period (from t_1 to t_2) as follows:

$$kNO_2 = \frac{HONO_{corr,t_2} - HONO_{corr,t_1}}{\overline{NO_2}(t_2 - t_1)} \quad (5)$$

where $\overline{NO_2}$ is the mean concentration of NO_2 between t_1 and t_2.

To evaluate the sensitivity of the results to the assumed emission factor, the calculation of $HONO_{corr}$ and k_{NO2} (**Fig. S3**) were calculated using emission factors of 0.005, 0.008 and 0.012 (Xu et al., 2015), while the observational inputs, analysis periods and calculation procedures held constant.

2.3 Machine learning technique

Random Forest (RF) algorithm, a machine learning technique extensively applied in atmospheric (Yang et al., 2024; Lin et al., 2026a; Zhang et al., 2025b), was employed to elucidate the primary drivers of kNO_2. The model was built using the "scikit-learn" library (https://github.com/scikit-learn/scikit-learn/blob/fe2edb3cd/sklearn/ensemble/, last access: June 10, 2026) in a python environment. Drawing upon previously identified factors influencing kNO_2 (e.g., pH, RH, NH_3) (Liu and Abbatt, 2021; Gen et al., 2024; Zhang et al., 2025a; Zhang et al., 2023) alongside the specific characteristics of the coastal urban environment, we incorporated meteorological parameters (RH and T), atmospheric reactive species (proxy of effective particle-phase chloride (Cl_{total}), NH_3, and NO_2), and heterogeneous-related parameters (pH, SA, and ground surfaces areas) as input variables for the RF model. Cl_{total} was defined as the sum of particulate Cl^- and gaseous HCl. It was used as a depletion-corrected proxy for the particulate Cl^- burden before acid displacement. During NO_2 uptake, the generated H^+ can protonate particulate Cl^- and release HCl to the gas phase. Consequently, measured particulate Cl^- represents the residual fraction after depletion, whereas HCl retains information about part of the chloride transferred from the particle phase. Their sum therefore represents, to some extent, the chloride burden before depletion. To evaluate the suitability of Cl_{total} as a proxy for the depletion-corrected Cl^- burden, two additional RF models were constructed by replacing Cl_{total} with either Cl^- or gaseous HCl. Variance inflation factors (VIFs) were calculated for the predictor set of each RF model. A VIF below 10 was used to

indicate the absence of severe multicollinearity. Only nighttime data were used to train the model to eliminate the effects of photochemical processes on kNO_2 quantification, thereby enabling a more precise identification of key drivers. Detailed RF hyperparameter configurations and model evaluation are provided in **Text S2**. In this study, the dominant factors were identified based on RF factor importance, which quantifies the percentage contribution of each variable to kNO_2 (Breiman, 2001; Gregorutti et al., 2017). Furthermore, one-dimensional partial dependence plots (PDPs) were employed to delineate the main effects of individual variables, while bivariate PDPs were utilized to visualize and access the interaction effects between pairs of factors on kNO_2 (Goldstein et al., 2015).

2.4 Multiphase chemical box model. The multiphase chemical box model was established based on the Framework for 0-D Atmospheric Modeling (F0AM) (Wolfe et al., 2016). As shown in **Table S1** and **Table S2**, comprehensive HONO and NO_3^- budgets were incorporated into the F0AM model to simulate the variations of HONO and NO_3^-. The ISORROPIA II model (Seinfeld et al., 1998) was integrated into the model to determine aerosol pH, aerosol liquid water content and the partitioning ratio of HNO_3 and NO_3^-. Six simulation scenarios were conducted: simulations without heterogeneous NO_2 uptake for (1) SLB and (2) non-SLB days; simulations with NO_2 uptake for (3) SLB and (4) non-SLB days, using the mean kNO_2 derived from SLB days for the SLB simulation and that derived from non-SLB days for the non-SLB simulation, respectively; and two additional sensitivity simulations for SLB days using the (5) 25th and (6) 75th percentiles of the kNO_2 distribution derived from SLB days. The ability of the model to reproduce real atmospheric processes was evaluated by comparing the simulated HONO and NO_3^- with observations. Due to the underestimation of total particulate nitrate concentrations measured by instruments, the performance of NO_3^- simulations was evaluated by comparing the trends of the simulated NO_3^- production rate with the observed NO_3^- concentration. In contrast, as HONO predominantly exists in the gas phase, the simulated HONO was evaluated directly against the observed HONO concentrations.

As for the model simulation, each simulation was preceded by a 3-day spin-up to allow intermediate species concentrations to stabilize. The mean diurnal pattern of trace gas concentrations, meteorological parameters, and the results from the ISORROPIA II model during SLB days and non-SLB days were used as input data to constrain the box model. Notably, the concentrations of HONO and NO_3^- were not constrained by observed values. More details about the model incorporating mechanisms, modules, and simulation settings are provided in **Text S3** and our previous study (Lin et al., 2026b).

3 Results and discussion

3.1 Characteristics of atmospheric species during SLB days

Fig. S1 shows the time series of the observed parameters. Based on the identification criteria detailed in the Methods section, 23 days were classified as SLB days, accounting for 48% of entire observation period. The diurnal patterns of major observed parameters are summarized in **Fig. S4**, revealing that the primary differences between the two types of days predominantly emerged at night. Compared to non-SLB days, SLB days exhibited rapid nighttime accumulation of HONO and NO_3^-, accompanied by elevated chlorine levels, NO_x concentrations, and aerosol surface area (SA) concentrations. Additionally, consistent with our previous study, SLB days were characterized by

higher temperature and RH at night (Chen et al., 2022). **Fig. 1** and **Table S3** further summarizes the nighttime observational results on SLB and non-SLB days. By definition, SLB days are influenced by persistent sea breezes, which likely enhances the impact of sea-salt aerosols. As shown in **Fig. 1a**, the Cl^- concentrations were comparatively higher on SLB days (0.154 μg/m^3) than on non-SLB days (0.139 μg/m^3). Specifically, this overall increase (**Fig. S5**) was primarily driven by elevated levels during the sea breeze (18:00-20:00 LT) and mixed sea-land breeze (21:00-00:00 LT) periods, while concentrations declined during the land breeze (01:00-06:00 LT) period. The elevation pattern of Cl^- indicates that the more abundant Cl^- transported by stronger sea breezes on SLB days can persist into the subsequent mixed sea-land breeze periods. Additionally, **Fig. S6** shows a moderate positive correlation between Na^+ and Cl^- on SLB days (r = 0.67), compared with a weaker relationship on non-SLB days (r = 0.28). Because sodium chloride (NaCl) is a major component of sea salt, this contrast is consistent with a greater sea-salt influence on Cl^- on SLB days. As for gaseous chlorine, **Fig. 1b** shows that the concentration of HCl was significantly higher on SLB days (96.2 ppt) than on non-SLB days (67.5 ppt). This further confirms that, under the influence of sea-salt aerosols on SLB days, chlorine levels are distinctly elevated in the nighttime coastal troposphere.

Fig. 1c indicates that the concentration of NO_2 on SLB days (mean: 28.3 ppb) was significantly higher than that on non-SLB days (23.2 ppb). Within our study area, ship emissions, cross-sea bridge traffic, and road traffic contribute substantial NO*x*, and the enhanced local circulation on SLB days can promote NO_2 accumulation (Chen et al., 2023). The mean concentrations of HONO and NO_3^- on SLB day were 0.836 ppb and 3.61 μg/m^3, respectively, which were significantly higher than the corresponding values of 0.497 ppb and 3.13 μg/m^3 on non-SLB days (**Figs. 1d-1e**). To better understand the elevated HONO levels, $HONO_{corr}$ concentrations, defined as the observed HONO concentration subtracts contributions from primary emissions and gas-phase production, were calculated to represent the nocturnal HONO produced from heterogeneous conversion. The ratio of $HONO_{corr}/NO_2$ was notably higher on SLB days (0.030) than on non-SLB days (0.021), indicating more active heterogeneous conversion of NO_2 to HONO on SLB days. Multiple studies have confirmed that NO_2 uptake is a primary source of nocturnal heterogeneous HONO formation (Zhang et al., 2023; Zhang et al., 2022). Here, the higher SA concentrations on SLB days were also conducive to heterogeneous reactions (**Fig. 1g**). Furthermore, **Figs. 2a-2b** indicate a moderate positive correlation between $HONO_{corr}$ and NO_3^-, with the correlation coefficient (r) increasing from 0.56 on non-SLB days to 0.76 on SLB days. The $HONO_{corr}$ concentrations under the two conditions overlapped mainly below 1.5 ppb. Within this overlapping range, the correlation on SLB days remained significant (r = 0.63, $p < 0.001$, **Fig. S7a**) but was close to that on non-SLB days (r = 0.56), indicating that the wider concentration range partly contributed to the higher full-range correlation on SLB days, while the positive relationship between $HONO_{corr}$ and NO_3^- persisted within the overlapping range. As shown in R1, NO_2 uptake via disproportionation simultaneously produces HONO and HNO_3, the latter of which is further converted to NO_3^- via gas-particle partitioning. Thus, nocturnal NO_2 uptake is also likely an important contributor to the formations of NO_3^- on SLB days. **Figs. 2c-2d** show that the full-range correlation between $HONO_{corr}$ and gaseous HCl was stronger on SLB days than on non-SLB days (r = 0.58 versus 0.16). Within the overlapping $HONO_{corr}$ range below 1.5 ppb, the correlation on SLB days decreased to (r = 0.47) but remained significant ($p <$ 0.001, **Fig. S7b**) and appreciably higher than that on non-SLB days. This result indicates that the stronger HCl-$HONO_{corr}$ relationship during SLB periods cannot be explained solely by the wider $HONO_{corr}$ range. The H^+ generated by NO_2 uptake can combine with Cl^- (R2-R3). Simultaneously,

the aerosol pH in the coastal region of southeastern China was relatively low (approximately 1.92 ± 0.34 during nocturnal SLB periods), chloride depletion could easily occur, leading to the observed positive correlation between $HONO_{corr}$ and HCl. The enhanced chloride depletion can also explain our observations of a significant increase in gaseous HCl but not in Cl^- concentrations on SLB days. Similarly, the rapid decline in Cl^- concentration during land breeze periods (**Fig. S4**) could also be explained by chloride depletion.

$$2NO_2 + H_2O(ad) + \text{aerosol/ground surface} \rightarrow HNO_3 + HONO \quad (R1)$$

$$NaCl(s) \rightarrow Na^+(aq) + Cl^-(aq) \quad (R2)$$

$$H^+(aq) + Cl^-(aq) \rightarrow HCl(aq) \leftrightharpoons HCl(g) \quad (R3)$$

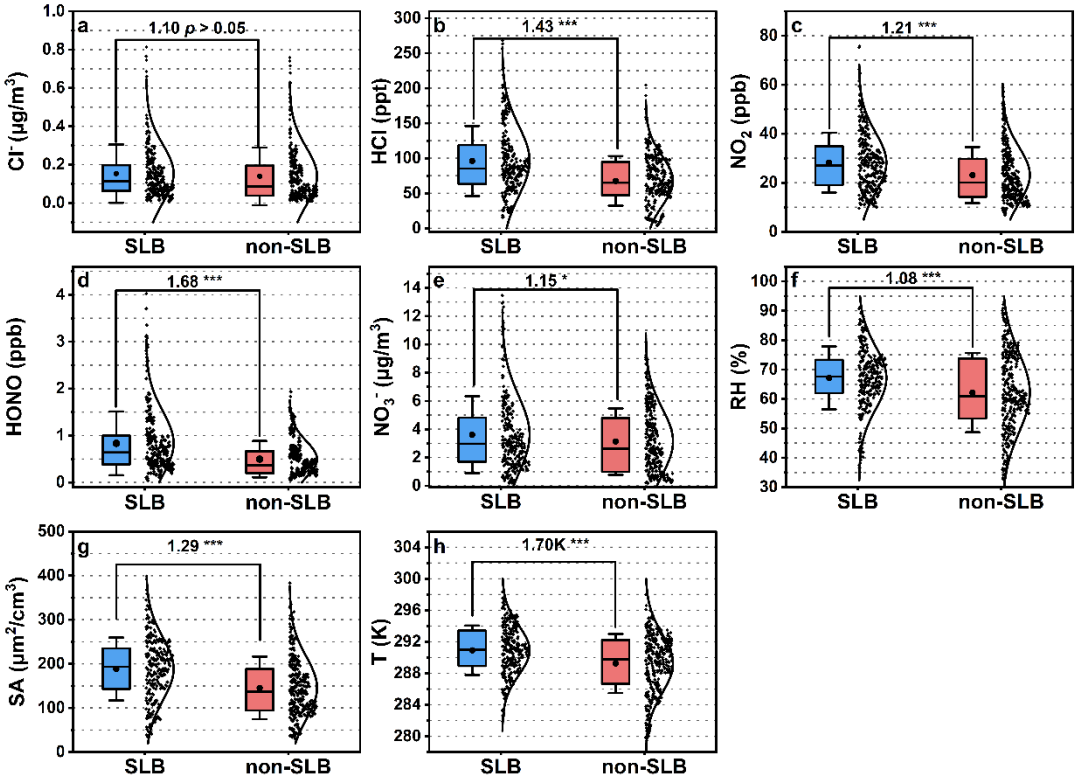

Figure 1. Box plots of key observed parameters during nocturnal SLB and non-SLB periods. (a) Cl^-, (b) HCl, (c) NO_2, (d) HONO, (e) NO_3^-, (f) RH, (g) SA, and (h) ambient temperature (T). The box shows the 25th–75th percentiles with whiskers representing ±1 standard deviation. The black dot and black line within the box represent the mean and the median. Differences between SLB and non-SLB days were tested using a two-sample t-test. Statistical significances are denoted as *(p < 0.05), **(p < 0.01) and ***(p < 0.001). For all panels except (h), the number adjacent to the significance symbol denotes the ratio of the mean value on SLB days to that on non-SLB days; in panel (h), it denotes the absolute difference between the means.

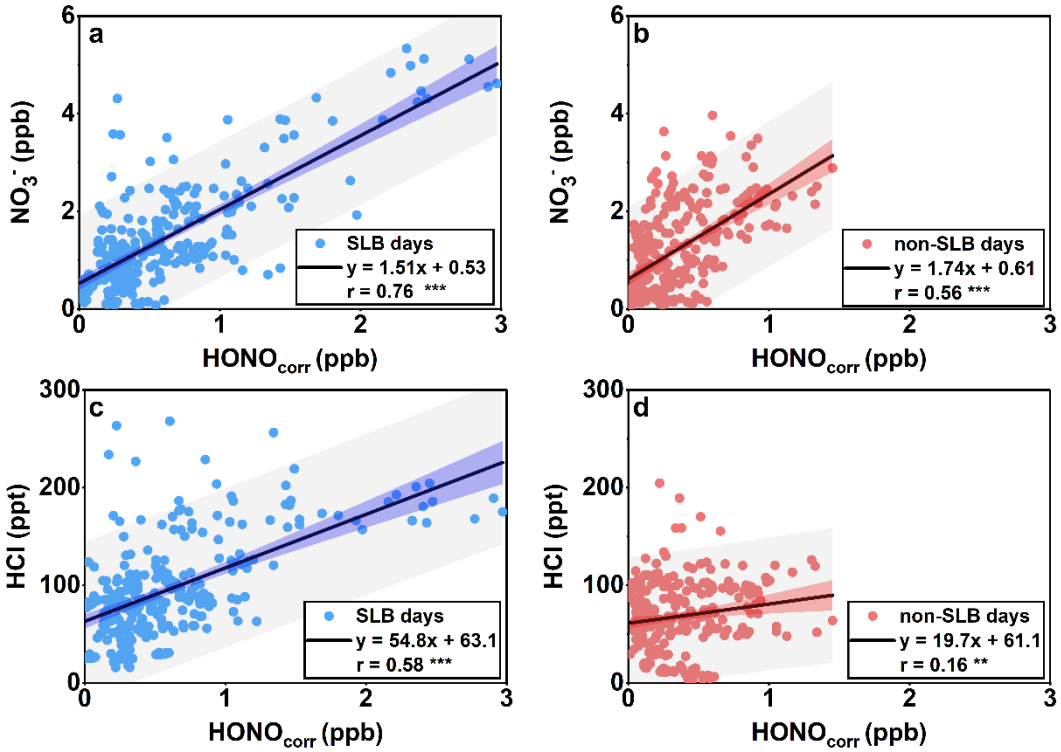

Figure 2. Relationship between $HONO_{corr}$ and the important products of heterogeneous chemical processes during nocturnal SLB and non-SLB periods. $HONO_{corr}$ denotes the corrected HONO concentration from secondary conversion. The products include (a, b) NO_3^- and (c, d) HCl. Blue and red dots represent observations during SLB days and non-SLB days, respectively. Each panel displays the linear regression fits and Pearson correlation coefficients (r) for the corresponding periods.

3.2 Enhanced rate of NO_2 uptake and its influencing factors

The values of kNO_2 on SLB days and non-SLB days were derived as **Fig. S8**. Overall, the average kNO_2 values on SLB days (9.70×10^{-6} s^{-1}) were significantly higher than those on non-SLB days (6.72×10^{-6} s^{-1}), by a factor of approximately 1.44. Across the tested emission factors, the mean $HONO_{corr}$ decreased from 0.58 to 0.51 ppb on SLB days, whereas kNO_2 varied by no more than 6.2%, indicating limited sensitivity of the derived rate constant to the assumed emission factor (**Fig. S3**). As presented in **Table S4**, a prolonged increase in the $HONO_{corr}/NO_2$ ratio was also observed during 17 of the 23 SLB days (see an example in **Fig. S9**). In contrast, this phenomenon was virtually absent on non-SLB days, indicating a sustained nocturnal enhancement of kNO_2 during SLB periods. Compared with existing field observations, the kNO_2 on SLB days was broadly consistent with the levels reported under the sea-case scenario in coastal cities of China such as Qingdao(1.25×10^{-5} s^{-1}) and Hong Kong(8.81×10^{-6} s^{-1}) (Yang et al., 2021; Zha et al., 2014), while it was markedly higher than those values observed in major non-coastal cities including Beijing (7.78×10^{-7} – 5.75×10^{-6} s^{-1}) (Wang et al., 2017b; Zhang et al., 2020; Xuan et al., 2023; Jia et al., 2020; Zhang et al., 2022), Nanjing (1.19×10^{-6} – 2.22×10^{-6} s^{-1}) (Zheng et al., 2020; Liu et al., 2019), and Guangzhou (4.44×10^{-6} – 6.67×10^{-6} s^{-1}) (Su et al., 2008; Li et al., 2012; Qin et al., 2009). The consistently higher kNO_2 in coastal areas implies that coastal atmospheric environments are likely more conducive to NO_2 uptake.

A machine learning technique was used to further identify key drivers of the enhanced kNO_2 on SLB days. The RF models using Cl_{total} reproduced the calculated kNO_2 well during both SLB and non-SLB periods, with R^2 values of 0.91 and 0.87, respectively (**Figs. S10c-10d**). Replacing Cl_{total} with either Cl^- or HCl resulted in the respective chlorine variable ranking third after RH and SA (**Fig. S10-S11**). Particulate Cl^- represents the residual particle-phase fraction, whereas HCl contains information on the fraction transferred to the gas phase through chloride depletion. Their respective importance therefore suggests that the Cl_{total} signal was not determined by either component alone, but reflected their complementary information on the Cl^- burden before depletion. All VIFs were below 10, indicating no severe multicollinearity between the chlorine metrics and the other predictors (**Table S5**). Because all three metrics retain part of the chlorine-related information, the RF models showed similar R^2 values (0.89 – 0.91); nevertheless, the Cl_{total}-based model had the highest R^2 and provided a more physically representative description of the association between depletion-corrected particulate chloride and kNO_2. Notably, the role of Cl_{total} and RH diminished substantially on non-SLB days (**Fig. 3b**), underscoring the profound modulation of these two influencing factors by the SLB circulation. **Fig 3c-3e** further elucidate the specific impacts of these primary drivers on nocturnal kNO_2 under SLB conditions. Specifically, Cl_{total} exhibits a positive correlation with kNO_2 (**Fig. 3c**). This phenomenon is likely attributable to the preferential partitioning of chloride ions at the gas-aqueous interface of aerosols (Zhang et al., 2025a; Shen et al., 2025; Wang et al., 2025a). The surface-bound Cl^- can attract gaseous NO_2 molecules (R4) to form interfacial intermediates $[Cl\text{-}NO_2]^-$, thereby facilitating the overall NO_2 uptake process. Subsequent interaction analysis was consistent with the mechanisms proposed in laboratory studies (R4-R5) and suggest that similar processes may operate in the coastal boundary layer. **Fig. 3f** shows that at a fixed NO_2 concentration, elevated chloride levels amplify the positive effect of NO_2 molecules on kNO_2. This indicates that chloride ions actively promote the heterogeneous uptake of NO_2, consequently accelerating the kNO_2. Similar halogen-promoted effect has also been revealed in NO_2-initiated aqueous-phase oxidation of dissolved SO_2 at the air-aqueous interface and of nitrate photolysis at the aqueous-phase surface (Wang et al., 2025a; Shen et al., 2025). **Fig. 3d** shows a significant positive relationship exists between RH and kNO_2, suggesting that moist sea breezes effectively supply the water molecules essential for the heterogeneous NO_2 uptake. This finding aligns with previously reported field observations highlighting RH-driven NO_2 uptake (Xuan et al., 2024). Analogous to Cl_{total}, the interaction between RH and NO_2 reveals that at a constant NO_2 level, the positive impact of NO_2 on kNO_2 is enhanced under elevated RH. It implies that RH could also facilitate NO_2 uptake by promoting the interaction between NO_2 molecules and heterogeneous interface. Furthermore, **Fig. 3h** shows a threshold-dependent joint enhancement: kNO_2 increased when RH exceeded approximately 80% and Cl_{total} exceeded approximately 0.5 $\mu g/m^3$, whereas the response was limited when either variable remained below these levels. Elevated RH can increase aerosol liquid water and maintain an aqueous particle phase, while Cl^- in wetted chloride-containing particles can be preferentially accessible at the air-aqueous interface and enhance NO_2 adsorption and uptake (Zhang et al., 2025a; Wang et al., 2025a). Therefore, the bivariate PDPs response is consistent with high RH providing a favorable aqueous interfacial environment for chloride-associated NO_2 uptake. This interaction may partly explain the higher importance of RH and Cl_{total} on SLB days. As a primary factor on both SLB and non-SLB days, SA positively correlates with kNO_2 (**Fig. 3e**). This indicates that an increase in aerosol surface area concentrations provides effective reaction interfaces for NO_2 uptake process, consistent with most atmospheric

heterogeneous processes (Wang et al., 2017a; Ma et al., 2026). Moreover, **Fig. S12** shows that on SLB days, concentrations of the major NO_2 uptake products (HONO and NO_3^-) increased with those key factors including Cl_{total}, RH, and SA, providing additional support for the above driving factor analysis. In general, the reasons underlying the enhanced kNO_2 on SLB days help to explain the multi-fold higher kNO_2 observed in coastal areas compared to non-coastal urban areas, highlighting ambient chlorine levels and RH as non-negligible contributors.

$$Cl^-(aq) + NO_2 \rightarrow [Cl\text{-}NO_2^-]_{surface} \quad (R4)$$

$$[Cl\text{-}NO_2^-]_{surface} + NO_2 + H_2O(ad) \rightarrow Cl^-(aq) + HONO + NO_3^- + H^+ \quad (R5)$$

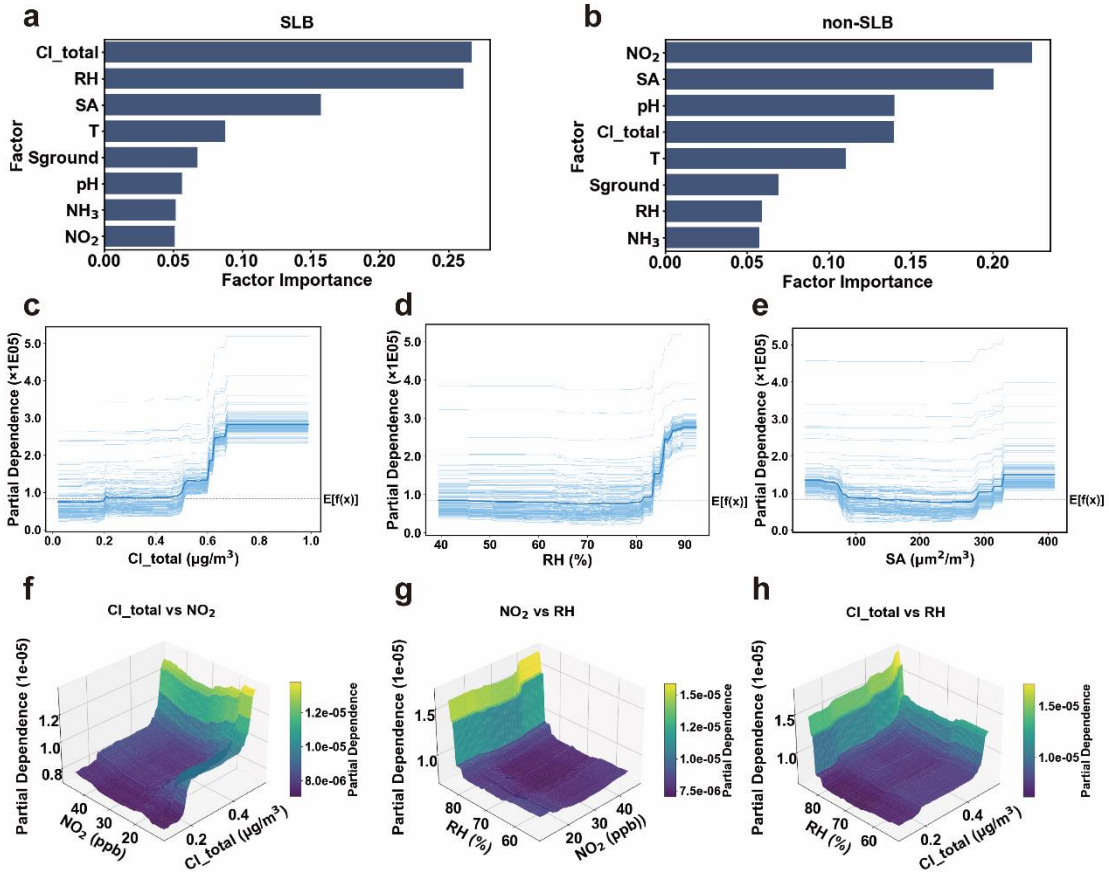

Figure 3. Main and interaction effects of influencing factors for k_{NO2}. Factor importance determined by the random forest (a) SLB days and (b) non-SLB days. Partial dependence plots for the primary drivers on SLB days: (c) Cl_{total}, (d) RH, and (e) SA. Interactions between key factors on SLB days: (f) Cl_{total} and NO_2, (g) RH and NO_2, and (h) RH and Cl_{total}. In panels (a-b), S_{ground} denotes ground surface areas calculated by 1/BLH (boundary layer height). In panels (c-h), partial dependence reflects the extent to which the influencing factors affect kNO_2.

3.3 Enhanced NO_2 uptake promotes the atmospheric reactive nitrogen cycle

The above correlations analysis suggests that NO_2 uptake could play an important role in the production of HONO and NO_3^- on SLB days. Since the HONO and NO_3^- formation were influenced by multiple meteorological factors and many atmospheric reaction pathways, a multiphase chemical box model was employed to evaluate the role of enhanced NO_2 uptake. As described in Methods, six simulation scenarios were set up. Incorporating NO_2 uptake mechanism substantially improved the simulated diurnal HONO profile during SLB periods: r increased from 0.57 to 0.94, while mean

absolute error (MAE) and root mean square error (RMSE) decreased from 0.58 to 0.11 ppb and from 0.64 to 0.13 ppb, respectively (**Fig. 4a**). For NO_3^-, incorporating NO_2 uptake increased the mean simulated net NO_3^- formation rate by 2.14 $\mu g/m^3/h$ and strengthened the temporal consistency between the simulated net formation rate and observed concentration, increasing r from 0.04 ($p > 0.05$) to 0.64 ($p < 0.001$, **Fig. 4b**). This improvement indicates that the added mechanism better represented the observed temporal variability in NO_3^- during SLB periods. Additionally, the NO_2 uptake could robustly explain the enhancements in both atmospheric reactive nitrogen species on SLB days across various kNO_2 quantiles (**Fig. S13**). In contrast, including NO_2 uptake under non-SLB conditions produced only limited improvements in the simulated HONO concentrations and the temporal covariation between NO_3^- production rates and observed NO_3^- concentrations (**Fig. S14**). This suggests that NO_2 uptake had less explanatory importance under non-SLB conditions than during SLB periods, consistent with the stronger observed $HONO_{corr}$-NO_3^- relationship on SLB days. Moreover, unlike on SLB days (**Fig. S9**), $HONO_{corr}/NO_2$ did not exhibit a sustained nocturnal increase on non-SLB days, which resulted in numerous negative estimates of kNO_2 estimated using Eq. (5). Excluding these negative values likely led to an overestimated mean kNO_2 and, consequently, to the overprediction of HONO and NO_3^- under non-SLB conditions.

Figs.4c-4d illustrate the simulated HONO and NO_3^- budgets for the scenarios incorporating NO_2 uptake on SLB days. Despite potential overestimations of non-SLB kNO_2, the mean NO_2 uptake rate remained significantly higher on SLB days than on non-SLB days, with an average rate of 1.03 ppb/h (**Fig. S15**). During nighttime, NO_2 uptake accounted for 83.8% of HONO formation (**Fig. 4e**). The predominance of NO_2 uptake in nocturnal HONO formation has also been observed during PM pollution episodes in urban areas (Xuan et al., 2024; Jia et al., 2020). However, unlike the chlorine-driven reason identified here, those prior cases were primarily attributed to favorable heterogeneous reaction conditions, such as larger SA concentrations, lower BLH, and higher RH. In addition to NO_2 uptake, primary emissions from vehicle exhaust, coal combustion, and biomass burning are also recognized as major contributors to nighttime HONO in urban areas (Wang et al., 2025b; Zhang et al., 2022). In this study, primary emissions contributed only 15.5% to nocturnal HONO formation, substantially less than the contribution from NO_2 uptake. As for nighttime NO_3^- formation, many studies had indicated that N_2O_5 uptake was the dominant pathway in urban areas (Chen et al., 2020; Wang et al., 2018). However, the situation changed under the impact of the enhanced NO_2 uptake. **Fig. 4f** shows that NO_2 uptake contributed 46.4% to nocturnal NO_3^- formation, which was almost comparable to that of N_2O_5 uptake (51.6%). These values were obtained using the BT09 parameterization of γN_2O_5 (Bertram and Thornton, 2009b). Additional simulations using the EJ05 and GRI09 schemes yielded contributions of 47.0–47.9% for NO_2 uptake and 50.0–50.9% for N_2O_5 uptake (**Fig. S16** and **Table S6**), indicating that their comparable importance was insensitive to the choice of γN_2O_5 parameterization (Evans and Jacob, 2005; Hallquist et al., 2003; Griffiths et al., 2009). While chlorine can also promote the uptake of N_2O_5 (Bertram and Thornton, 2009a), the relative enhancement in the contribution of NO_2 uptake to nocturnal NO_3^- formation was more pronounced. This might be related to the suppression of N_2O_5 uptake caused by increased NO_3^- generating directly from NO_2 uptake. The increase in NO_3^- component of aerosol can shift the equilibrium between N_2O_5 and NO_3^- toward N_2O_5, thereby reducing the contribution of N_2O_5 to NO_3^- formation (Bertram and Thornton, 2009a; Wagner et al., 2013). Additionally, the enhanced NO_2 uptake process also competed for NO_2, an important precursor of N_2O_5 formation, especially in the NO_2-limited regime for N_2O_5 formation (Lin et al.,

2025), ultimately reducing the overall enhancement effect on N_2O_5 generation. Moreover, this comparable contribution of NO_2 and N_2O_5 uptake NO_3^- formation was also found during fog events (Xu et al., 2024). Although the observed phenomenon was similar, the dominant drivers differed between fog conditions and coastal SLB periods. The former was primarily attributed to favorable uptake conditions such as abundant aerosol water content and high surface area concentration, whereas the latter was more due to the enhancement effect of chlorine levels and RH on the NO_2 uptake process. Overall, these results reveal the high contribution of NO_2 uptake to HONO and NO_3^- formation during SLB circulation periods, demonstrating that enhanced NO_2 uptake can significantly influence the atmospheric reactive nitrogen cycle in coastal urban areas.

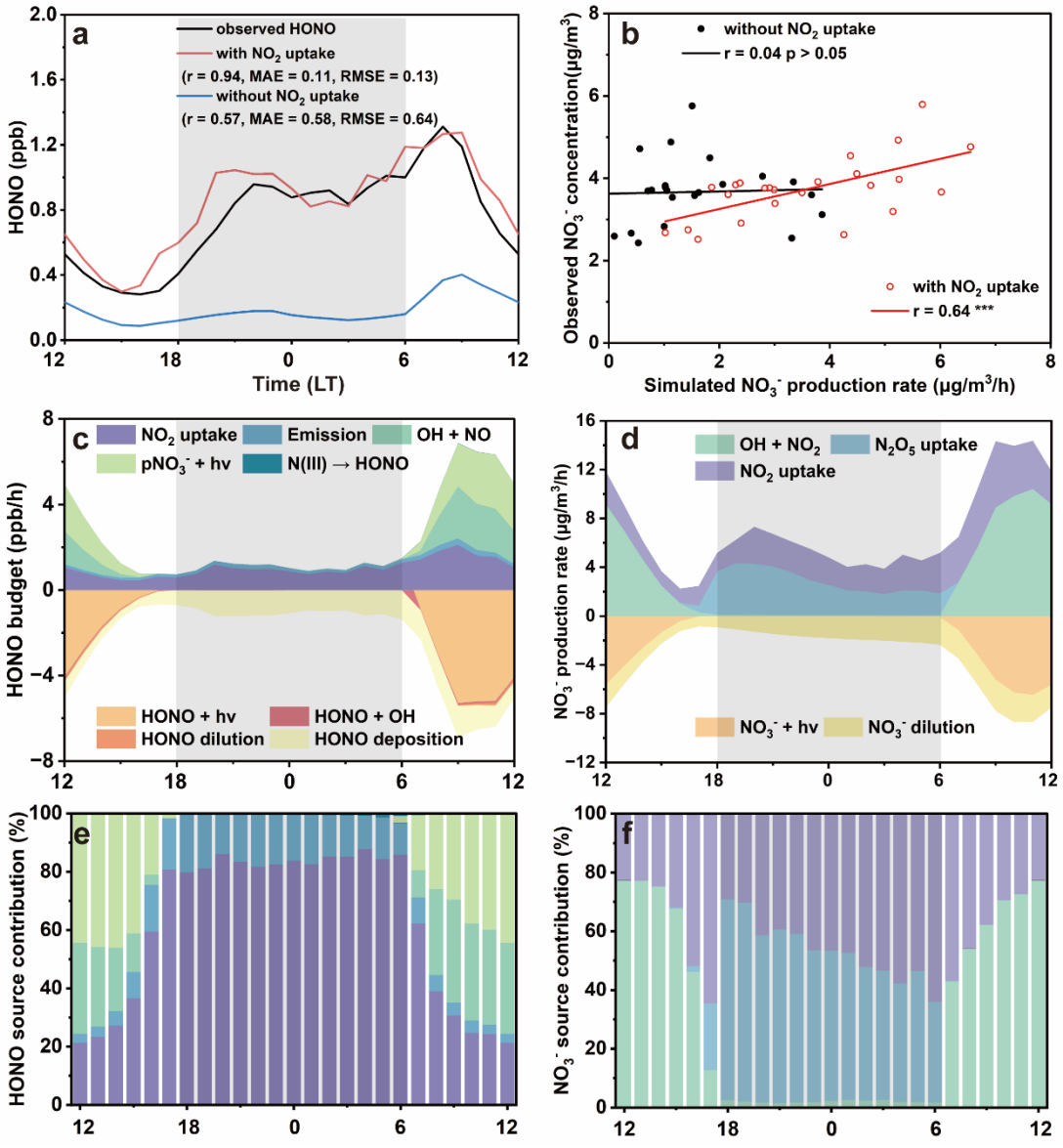

Figure 4. Quantified results from the multiphase chemical box model during SLB periods. (a) Diurnal variations in observed and simulated HONO concentrations with and without NO_2 uptake. (b) Relationship between the simulated NO_3^- production rate and observed concentration with and without NO_2 uptake. Diurnal variations of HONO (c) and NO_3^- budgets (d) during SLB days. Diurnal variations of source contributions to (e) HONO and (f) NO_3^-. The grey shaded areas represent the nighttime period.

4. Conclusions

Overall, our observations show that nighttime sea-land breeze period in this coastal urban site were characterized by stronger sea-salt aerosol influence, higher relative humidity, and elevated HONO and nitrate concentrations. Nighttime conditions led to a significant enhancement in the NO_2 uptake rate constant, mainly driven by increased chlorine levels and relative humidity. Multiphase chemical box model simulations further confirmed that this enhanced NO_2 uptake promoted HONO and nitrate formation. **Fig.5** illustrates a schematic diagram of chlorine-enhanced heterogeneous uptake of NO_2 during sea-land breeze days. Under the influence of strong sea-land breeze circulation, the continuous influx of sea-salt aerosols transported by moist sea breezes leads to high chlorine levels during the night. Meanwhile, emission from vehicles and ships contribute substantial NO_2, which accumulates in the coastal atmospheric boundary layer (Wen et al., 2023; Sun et al., 2025). Under these conditions, abundant chloride can effectively increase kNO_2 and promote the NO_2 uptake process, thereby influencing the formation of key atmospheric reactive nitrogen species, HONO and NO_3^-, as well as broader reactive nitrogen cycling. Notably, other sea-salt halides (Br^-, I^-) exhibit similar chemical properties to chlorine and may also contribute to the elevated kNO_2 (Zhang et al., 2025a).

Although the observations were limited to one coastal urban site in autumn and winter, chlorine-enhanced NO_2 uptake may also occur in other coastal environments where chloride-rich sea-salt aerosols, high RH, and sufficient NO_2 coexist. Its magnitude is expected to vary seasonally and regionally with sea-salt loading, aerosol water content, aerosol composition, and NO_2 abundance. Therefore, the quantitative contribution derived here should be considered site- and period-specific, and multi-season observations at other coastal sites are needed to assess its broader relevance. Additionally, our study focuses specifically on nocturnal NO_2 uptake to form HONO, given that daytime HONO formation involves more complex factors such as photo-enhanced heterogeneous reactions of NO_2 and nitrate photolysis (Stemmler et al., 2006; Han et al., 2016; Ye et al., 2017; Zhou et al., 2011). Future investigations are warranted to explicitly evaluate the impact of chlorine on daytime NO_2 uptake. Moreover, current air quality models often exhibit considerable biases in simulating secondary pollutants such as O_3 and $PM_{2.5}$ over coastal areas (Huang et al., 2025; Ma et al., 2025; Mao et al., 2022). One possible reason is that the influence of chlorine on chemical processes like NO_2 uptake has not yet been adequately considered. Given the dense traffic and substantial NO_2 emission in coastal cities of China, greater attention should be paid to the chlorine-enhanced NO_2 uptake process and its subsequent impact on nocturnal chemistry in coastal urban atmosphere.

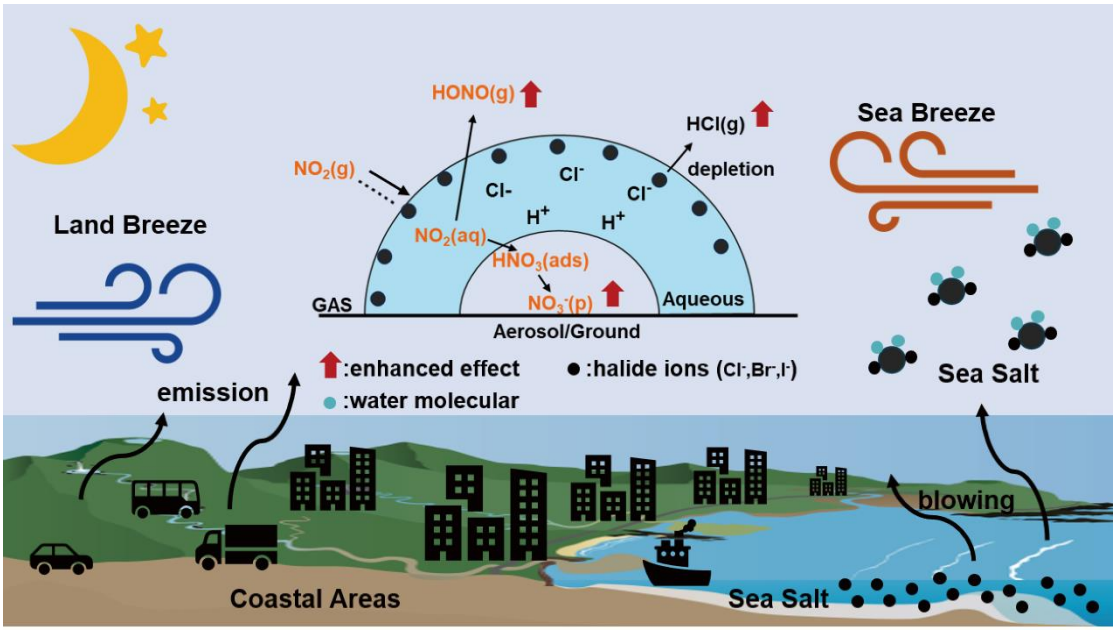

Figure 5. Schematic of the chlorine-enhanced heterogeneous uptake of NO_2 during sea-land breeze days in coastal areas. Red arrows, black solid circles, and blue solid circles represent the enhancement of the uptake process, halide ions and water molecular, respectively.

Code availability. Data analysis methods are available on request from Jinsheng Chen (jschen@iue.ac.cn).

Data availability. The dataset can be accessed at Zenodo website (Lin et al., 2026).

Author contributions:

Z.L. contributed to the conceptualization, investigation, methodology, data curation, software, analysis and writing of the original draft. L.X. and J.C. contributed to the data curation, reviewing and editing the text, supervision, and funding acquisition. X.Y., L.L., C.Y., X.J., Y.C., K.Z., F.Z., Z.C., G.C., X.F., and M.L. provided useful advice and revised the manuscript.

Competing interests:

The authors declare no competing interests.

Acknowledgements. The authors acknowledge all members of the atmospheric chemistry team at the Institute of Urban Environment.

Financial support. This work was funded by the National Natural Science Foundation of China (42677128 & U22A20578), the guiding project of seizing the commanding heights of "self-purifying city" (IUE-CERAE-202402), the National Key Research and Development Program (2022YFC3700304), STS Plan Supporting Project of the Chinese Academy of Sciences in Fujian Province (2023T3013), and Xiamen Atmospheric Environment Observation and Research Station of Fujian Province.

References:

Acker, K., Möller, D., Wieprecht, W., Meixner, F. X., Bohn, B., Gilge, S., Plass-Dülmer, C., and Berresheim, H.: Strong daytime production of OH from HNO_2 at a rural mountain site, Geophysical Research Letters. 33, https://doi.org/10.1029/2005GL024643, 2006.

Alicke, B., Geyer, A., Hofzumahaus, A., Holland, F., Konrad, S., Pätz, H. W., Schäfer, J., Stutz, J., Volz-Thomas, A., and Platt, U.: OH formation by HONO photolysis during the BERLIOZ experiment, Journal of Geophysical Research: Atmospheres. 108, PHO 3-1-PHO 3-17, https://doi.org/ 10.1029/2001JD000579, 2003.

Bertram, T. H. and Thornton, J. A.: Toward a general parameterization of N_2O_5 reactivity on aqueous particles: the competing effects of particle liquid water, nitrate and chloride, Atmos. Chem. Phys., 9, 8351-8363, https://doi.org/10.5194/acp-9-8351-2009, 2009a.

Bertram, T. H. and Thornton, J. A.: Toward a general parameterization of N_2O_5 reactivity on aqueous particles: the competing effects of particle liquid water, nitrate and chloride, Atmos. Chem. Phys., 9, 8351-8363, https://doi.org/10.5194/acp-9-8351-2009, 2009b.

Breiman, L.: Random Forests, Machine Learning. 45, 5-32, https://doi.org/10.1023/A:1010933404324, 2001.

Cao, Y., Ma, Q., Chu, B., and He, H.: Homogeneous and heterogeneous photolysis of nitrate in the atmosphere: state of the science, current research needs, and future prospects, Frontiers of Environmental Science & Engineering. 17, 48, https://doi.org/10.1007/s11783-023-1648-6, 2022.

Carter, W. P. L., Atkinson, R., Winer, A. M., and Pitts Jr, J. N.: Experimental investigation of chamber-dependent radical sources, International Journal of Chemical Kinetics. 14, 1071-1103, https://doi.org/10.1002/kin.550141003, 1982.

Chen, X., Wang, H., Lu, K., Li, C., Zhai, T., Tan, Z., Ma, X., Yang, X., Liu, Y., Chen, S., Dong, H., Li, X., Wu, Z., Hu, M., Zeng, L., and Zhang, Y.: Field Determination of Nitrate Formation Pathway in Winter Beijing, Environmental Science & Technology. 54, 9243-9253, https://doi.org/10.1021/acs.est.0c00972, 2020.

Chen, Y., Yang, C., Xu, L., Chen, J., Zhang, Y., Shi, J., Fan, X., Zheng, R., Hong, Y., and Li, M.: Chemical composition of NR-PM1 in a coastal city of Southeast China: Temporal variations and formation pathways, Atmospheric Environment. 285, 119243, https://doi.org/ 10.1016/j.atmosenv.2022.119243, 2022.

Chen, Y., Yang, C., Xu, L., Fan, X., Shi, J., Zheng, R., Hong, Y., Li, M., Liu, T., Chen, G., Yin, L., and Chen, J.: Variations of chemical composition of NR-PM_1 under the influence of sea land breeze in a coastal city of Southeast China, Atmospheric Research. 285, 106626, https://doi.org/ 10.1016/j.atmosres.2023.106626, 2023.

Cui, L., Li, R., Zhang, Y., Meng, Y., Fu, H., and Chen, J.: An observational study of nitrous acid (HONO) in Shanghai, China: The aerosol impact on HONO formation during the haze episodes, Science of The Total Environment. 630, 1057-1070, https://doi.org/10.1016/j.scitotenv.2018.02.063, 2018.

Evans, M. J. and Jacob, D. J.: Impact of new laboratory studies of N_2O_5 hydrolysis on global model budgets of tropospheric nitrogen oxides, ozone, and OH, Geophysical Research Letters. 32, https://doi.org/10.1029/2005GL022469, 2005.

Gen, M., Zheng, H., Sun, Y., Xu, W., Ma, N., Su, H., Cheng, Y., Wang, S., Xing, J., Zhang, S., Xue, L., Xue, C., Mu, Y., Tian, X., Matsuki, A., and Song, S.: Rapid hydrolysis of NO_2 at High Ionic Strengths of Deliquesced Aerosol Particles, Environmental Science & Technology. 58, 7904-7915, https://doi.org/10.1021/acs.est.3c08810, 2024.

Goldstein, A., Kapelner, A., Bleich, J., and Pitkin, E.: Peeking Inside the Black Box: Visualizing Statistical Learning With Plots of Individual Conditional Expectation, Journal of Computational and Graphical Statistics. 24, 44-65, https://doi.org/10.1080/10618600.2014.907095, 2015.

Gregorutti, B., Michel, B., and Saint-Pierre, P.: Correlation and variable importance in random forests, Statistics and Computing. 27, 659-678, https://doi.org/10.1007/s11222-016-9646-1, 2017.

Griffiths, P. T., Badger, C. L., Cox, R. A., Folkers, M., Henk, H. H., and Mentel, T. F.: Reactive Uptake of N_2O_5 by Aerosols Containing Dicarboxylic Acids. Effect of Particle Phase, Composition, and Nitrate Content, The Journal of Physical Chemistry A. 113, 5082-5090, https://doi.org/10.1021/jp8096814, 2009.

Hallquist, M., Stewart, D. J., Stephenson, S. K., and Anthony Cox, R.: Hydrolysis of N_2O_5 on sub-micron sulfate aerosols, Physical Chemistry Chemical Physics. 5, 3453-3463, https://doi.org/10.1039/B301827J, 2003.

Han, C., Yang, W., Wu, Q., Yang, H., and Xue, X.: Heterogeneous Photochemical Conversion of NO_2 to HONO on the Humic Acid Surface under Simulated Sunlight, Environmental Science & Technology. 50, 5017-5023, https://doi.org/10.1021/acs.est.5b05101, 2016.

Hao, Q., Jiang, N., Zhang, R., Yang, L., and Li, S.: Characteristics, sources, and reactions of nitrous acid during winter at an urban site in the Central Plains Economic Region in China, Atmos. Chem. Phys., 20, 7087-7102, https://doi.org/10.5194/acp-20-7087-2020, 2020.

Hersbach, H., Bell, B., Berrisford, P., Hirahara, S., Horányi, A., Muñoz-Sabater, J., Nicolas, J., Peubey, C., Radu, R., Schepers, D., Simmons, A., Soci, C., Abdalla, S., Abellan, X., Balsamo, G., Bechtold, P., Biavati, G., Bidlot, J., Bonavita, M., De Chiara, G., Dahlgren, P., Dee, D., Diamantakis, M., Dragani, R., Flemming, J., Forbes, R., Fuentes, M., Geer, A., Haimberger, L., Healy, S., Hogan, R. J., Hólm, E., Janisková, M., Keeley, S., Laloyaux, P., Lopez, P., Lupu, C., Radnoti, G., de Rosnay, P., Rozum, I., Vamborg, F., Villaume, S., and Thépaut, J.-N.: The ERA5 global reanalysis, Quarterly Journal of the Royal Meteorological Society. 146, 1999-2049, https://doi.org/ 10.1002/qj.3803, 2020.

Huang, L., Zhang, X., Emery, C., Mu, Q., Yarwood, G., Zhai, H., Sun, Z., Xue, S., Wang, Y., Fu, J. S., and Li, L.: Recommendations on benchmarks for numerical air quality model applications in China – Part 2: Ozone and uncertainty analysis, Atmos. Chem. Phys., 25, 4233-4249, https://doi.org/10.5194/acp-25-4233-2025, 2025.

Jia, C., Tong, S., Zhang, W., Zhang, X., Li, W., Wang, Z., Wang, L., Liu, Z., Hu, B., Zhao, P., and Ge, M.: Pollution characteristics and potential sources of nitrous acid (HONO) in early autumn 2018 of Beijing, Science of The Total Environment. 735, 139317, https://doi.org/ 10.1016/j.scitotenv.2020.139317, 2020.

Jungwirth, P. and Tobias, D. J.: Specific Ion Effects at the Air/Water Interface, Chemical Reviews. 106, 1259-1281, https://doi.org/10.1021/cr0403741, 2006.

Kleffmann, J., Kurtenbach, R., Lörzer, J., Wiesen, P., Kalthoff, N., Vogel, B., and Vogel, H.: Measured and simulated vertical profiles of nitrous acid—Part I: Field measurements, Atmospheric Environment. 37, 2949-2955, https://doi.org/10.1016/S1352-2310(03)00242-5, 2003.

Knipping, E. M., Lakin, M. J., Foster, K. L., Jungwirth, P., Tobias, D. J., Gerber, R. B., Dabdub, D., and Finlayson-Pitts, B. J.: Experiments and Simulations of Ion-Enhanced Interfacial Chemistry on Aqueous NaCl Aerosols, Science. 288, 301-306, https://doi.org/10.1126/science.288.5464.301, 2000.

Kulmala, M., Petäjä, T., Nieminen, T., Sipilä, M., Manninen, H. E., Lehtipalo, K., Dal Maso, M.,

585 Aalto, P. P., Junninen, H., Paasonen, P., Riipinen, I., Lehtinen, K. E. J., Laaksonen, A., and Kerminen,
586 V.-M.: Measurement of the nucleation of atmospheric aerosol particles, Nature Protocols. 7, 1651-
587 1667, https://doi.org/10.1038/nprot.2012.091, 2012.
588 Lee, Y. N. and Schwartz, S. E.: Reaction kinetics of nitrogen dioxide with liquid water at low partial
589 pressure, The Journal of Physical Chemistry. 85, 840-848, https://doi.org/10.1021/j150607a022,
590 1981.
591 Li, L., Lin, Z., Li, M., Fan, X., Yang, C., Hou, A., Chen, Y., Xu, L., Hong, Y., and Chen, J.:
592 Importance of Methanesulfonic Acid in New Particle Formation in a Coastal City of Southeast China,
593 Geophysical Research Letters. 52, e2025GL117238, https://doi.org/10.1029/2025GL117238, 2025.
594 Li, X., Brauers, T., Häseler, R., Bohn, B., Fuchs, H., Hofzumahaus, A., Holland, F., Lou, S., Lu, K.
595 D., Rohrer, F., Hu, M., Zeng, L. M., Zhang, Y. H., Garland, R. M., Su, H., Nowak, A., Wiedensohler,
596 A., Takegawa, N., Shao, M., and Wahner, A.: Exploring the atmospheric chemistry of nitrous acid
597 (HONO) at a rural site in Southern China, Atmos. Chem. Phys., 12, 1497-1513,
598 https://doi.org/10.5194/acp-12-1497-2012, 2012.
599 Lin, Z., Li, L., Xu, L., Ji, X., Zhang, K., Yang, C., Chen, G., Fan, X., and Chen, J.: Unexpected
600 Daytime N_2O_5 in Urban Areas: Formation Mechanisms and Environmental Impacts, Geophysical
601 Research Letters. 53, e2025GL121461, https://doi.org/10.1029/2025GL121461, 2026a.
602 Lin, Z., Ji, X., Xu, L., Chen, G., Yang, C., Zhang, K., Zhang, F., Li, L., Chen, Y., and Chen, J.:
603 Enhanced NO_2-driven multiphase formation of particulate nitrate and sulfate under high-humidity
604 conditions, npj Climate and Atmospheric Science. 9, 76, https://doi.org/10.1038/s41612-026-
605 01352-5, 2026b.
606 Lin, Z., Ying, C., Xu, L., Ji, X., Zhang, K., Zhang, F., Chen, G., Li, L., Yang, C., Chen, Y., Chen, Z.,
607 and Chen, J.: Measurement report: High contribution of N_2O_5 uptake to particulate nitrate formation
608 in NO2-limited urban areas, Atmos. Chem. Phys., 25, 17747-17759, https://doi.org/10.5194/acp-25-
609 17747-2025, 2025.
610 Liu, C., Wang, H., Li, L., Chen, X., Lu, X., and Fan, S.: Impacts of sea-land breeze on the coastal
611 ozone in the Pearl River Delta, China, Journal of Environmental Sciences.
612 https://doi.org/10.1016/j.jes.2025.08.037, 2025.
613 Liu, T. and Abbatt, J. P. D.: Oxidation of sulfur dioxide by nitrogen dioxide accelerated at the
614 interface of deliquesced aerosol particles, Nature Chemistry. 13, 1173-1177,
615 https://doi.org/10.1038/s41557-021-00777-0, 2021.
616 Liu, T., Hong, Y., Li, M., Xu, L., Chen, J., Bian, Y., Yang, C., Dan, Y., Zhang, Y., Xue, L., Zhao, M.,
617 Huang, Z., and Wang, H.: Atmospheric oxidation capacity and ozone pollution mechanism in a
618 coastal city of southeastern China: analysis of a typical photochemical episode by an observation-
619 based model, Atmos. Chem. Phys., 22, 2173-2190, https://doi.org/10.5194/acp-22-2173-2022, 2022.
620 Liu, Y., Nie, W., Xu, Z., Wang, T., Wang, R., Li, Y., Wang, L., Chi, X., and Ding, A.: Semi-
621 quantitative understanding of source contribution to nitrous acid (HONO) based on 1 year of
622 continuous observation at the SORPES station in eastern China, Atmos. Chem. Phys., 19, 13289-
623 13308, https://doi.org/10.5194/acp-19-13289-2019, 2019.
624 Ma, W., Chen, X., Wang, Y., Zhang, Y., Zheng, F., Li, J., Hua, C., Zhao, Z., Yuan, Q., Wu, J., Jiang,
625 J., Ye, P., Kulmala, M., Worsnop, D. R., Yang, H., and Liu, Y.: High Aerosol Ionic Strength Possibly
626 Affecting Nocturnal Chlorine Formation via Heterogeneous Reaction in Urban Beijing,
627 Environmental Science & Technology. 60, 902-912, https://doi.org/10.1021/acs.est.5c09187, 2026.
628 Ma, X., Liu, H., and Peng, Z.: Improving $PM_{2.5}$ and PM_{10} predictions in China from WRF Chem

through a deep learning method: Multiscale depth-separable UNet, Environmental Pollution. 364, 125344, https://doi.org/10.1016/j.envpol.2024.125344, 2025.
Mao, J., Li, L., Li, J., Sulaymon, I. D., Xiong, K., Wang, K., Zhu, J., Chen, G., Ye, F., Zhang, N., Qin, Y., Qin, M., and Hu, J.: Evaluation of Long-Term Modeling Fine Particulate Matter and Ozone in China During 2013–2019, Frontiers in Environmental Science. Volume 10 - 2022, https://doi.org/10.3389/fenvs.2022.872249, 2022.
Nie, W., Yan, C., Huang, D. D., Wang, Z., Liu, Y., Qiao, X., Guo, Y., Tian, L., Zheng, P., Xu, Z., Li, Y., Xu, Z., Qi, X., Sun, P., Wang, J., Zheng, F., Li, X., Yin, R., Dallenbach, K. R., Bianchi, F., Petäjä, T., Zhang, Y., Wang, M., Schervish, M., Wang, S., Qiao, L., Wang, Q., Zhou, M., Wang, H., Yu, C., Yao, D., Guo, H., Ye, P., Lee, S., Li, Y. J., Liu, Y., Chi, X., Kerminen, V.-M., Ehn, M., Donahue, N. M., Wang, T., Huang, C., Kulmala, M., Worsnop, D., Jiang, J., and Ding, A.: Secondary organic aerosol formed by condensing anthropogenic vapours over China's megacities, Nature Geoscience. 15, 255-261, https://doi.org/10.1038/s41561-022-00922-5, 2022.
Piatkowski, L., Zhang, Z., Backus, E. H. G., Bakker, H. J., and Bonn, M.: Extreme surface propensity of halide ions in water, Nature Communications. 5, 4083, https://doi.org/10.1038/ncomms5083, 2014.
Qin, M., Xie, P., Su, H., Gu, J., Peng, F., Li, S., Zeng, L., Liu, J., Liu, W., and Zhang, Y.: An observational study of the HONO–NO_2 coupling at an urban site in Guangzhou City, South China, Atmospheric Environment. 43, 5731-5742, https://doi.org/10.1016/j.atmosenv.2009.08.017, 2009.
Qu, R. and Han, G.: A critical review of the variation in rainwater acidity in 24 Chinese cities during 1982–2018, Elementa: Science of the Anthropocene. 9, 00142, https://doi.org/10.1525/elementa.2021.00142, 2021.
Seinfeld, J. H., Pandis, S. N., and Noone, K. J.: Atmospheric Chemistry and Physics: From Air Pollution to Climate Change, Physics Today. 51, 88-90, 1998.
Shen, H., Li, Q., Xu, F., Xue, L., Hu, Y., Saiz-Lopez, A., Wang, W., and Wang, T.: Aerosol iodide accelerates reactive nitrogen cycling in the marine atmosphere, Nature Communications. 16, 8148, https://doi.org/10.1038/s41467-025-63420-3, 2025.
Shi, X., Ge, Y., Zheng, J., Ma, Y., Ren, X., and Zhang, Y.: Budget of nitrous acid and its impacts on atmospheric oxidative capacity at an urban site in the central Yangtze River Delta region of China, Atmospheric Environment. 238, 117725, https://doi.org/10.1016/j.atmosenv.2020.117725, 2020.
Stemmler, K., Ammann, M., Donders, C., Kleffmann, J., and George, C.: Photosensitized reduction of nitrogen dioxide on humic acid as a source of nitrous acid, Nature. 440, 195-198, https://doi.org/10.1038/nature04603, 2006.
Su, H., Cheng, Y. F., Cheng, P., Zhang, Y. H., Dong, S., Zeng, L. M., Wang, X., Slanina, J., Shao, M., and Wiedensohler, A.: Observation of nighttime nitrous acid (HONO) formation at a non-urban site during PRIDE-PRD2004 in China, Atmospheric Environment. 42, 6219-6232, https://doi.org/10.1016/j.atmosenv.2008.04.006, 2008.
Sun, L., Zhang, J., Ducruet, C., Itoh, H., and Liu, X.: The impact of shipping activities on air quality and residents' health in China's port cities, Journal of Transport Geography. 123, 104099, https://doi.org/10.1016/j.jtrangeo.2024.104099, 2025.
Wagner, N. L., Riedel, T. P., Young, C. J., Bahreini, R., Brock, C. A., Dubé, W. P., Kim, S., Middlebrook, A. M., Öztürk, F., Roberts, J. M., Russo, R., Sive, B., Swarthout, R., Thornton, J. A., VandenBoer, T. C., Zhou, Y., and Brown, S. S.: N_2O_5 uptake coefficients and nocturnal NO_2 removal rates determined from ambient wintertime measurements, Journal of Geophysical Research:

Atmospheres. 118, 9331-9350, https://doi.org/10.1002/jgrd.50653, 2013.
Wang, G., Zhang, S., Wu, C., Zhu, T., Xu, X., Ge, S., Sun, H., Sun, Z., Wang, J., Ji, Y., Gao, J., Ren, Y., Li, H., Zhang, F., Wang, Y., and Seinfeld, J. H.: Atmospheric sulfate aerosol formation enhanced by interfacial anions, PNAS Nexus. 4, pgaf058, https://doi.org/10.1093/pnasnexus/pgaf058, 2025a.
Wang, H., Lu, K., Guo, S., Wu, Z., Shang, D., Tan, Z., Wang, Y., Le Breton, M., Lou, S., Tang, M., Wu, Y., Zhu, W., Zheng, J., Zeng, L., Hallquist, M., Hu, M., and Zhang, Y.: Efficient N_2O_5 uptake and NO_3 oxidation in the outflow of urban Beijing, Atmos. Chem. Phys., 18, 9705-9721, https://doi.org/10.5194/acp-18-9705-2018, 2018.
Wang, H., Lu, K., Chen, X., Zhu, Q., Chen, Q., Guo, S., Jiang, M., Li, X., Shang, D., Tan, Z., Wu, Y., Wu, Z., Zou, Q., Zheng, Y., Zeng, L., Zhu, T., Hu, M., and Zhang, Y.: High N_2O_5 Concentrations Observed in Urban Beijing: Implications of a Large Nitrate Formation Pathway, Environmental Science & Technology Letters. 4, 416-420, https://doi.org/10.1021/acs.estlett.7b00341, 2017a.
Wang, J., Zhang, X., Guo, J., Wang, Z., and Zhang, M.: Observation of nitrous acid (HONO) in Beijing, China: Seasonal variation, nocturnal formation and daytime budget, Science of The Total Environment. 587-588, 350-359, https://doi.org/10.1016/j.scitotenv.2017.02.159, 2017b.
Wang, Y., Liu, P., Zhang, C., Xue, C., Zhao, X., Fu, S., Wu, Z., Song, Y., Wang, Y., Liu, C., and Mu, Y.: Evaluating the contribution of residential coal combustion to atmospheric nitrous acid (HONO) in winter, Environmental Pollution. 378, 126488, https://doi.org/10.1016/j.envpol.2025.126488, 2025b.
Wen, Y., Liu, M., Zhang, S., Wu, X., Wu, Y., and Hao, J.: Updating On-Road Vehicle Emissions for China: Spatial Patterns, Temporal Trends, and Mitigation Drivers, Environmental Science & Technology. 57, 14299-14309, https://doi.org/10.1021/acs.est.3c04909, 2023.
Wentzell, J. J. B., Schiller, C. L., and Harris, G. W.: Measurements of HONO during BAQS-Met, Atmos. Chem. Phys., 10, 12285-12293, https://doi.org/10.5194/acp-10-12285-2010, 2010.
Wolfe, G. M., Marvin, M. R., Roberts, S. J., Travis, K. R., and Liao, J.: The Framework for 0-D Atmospheric Modeling (F0AM) v3.1, Geosci. Model Dev., 9, 3309-3319, https://doi.org/10.5194/gmd-9-3309-2016, 2016.
Xie, J., Sun, J., Li, Y., Chan, P. W., Li, L., Huang, C., Tang, L., Fan, S., Zheng, Y., and Fan, Z.: Sea-land breezes in the Guangdong- Hong Kong- Macau Greater Bay Area coastal zone from 2013 to 2022, Atmospheric Research. 296, 107044, https://doi.org/10.1016/j.atmosres.2023.107044, 2023.
Xu, W., Kuang, Y., Xu, W., Liu, L., Xu, H., Wang, X., Liu, Y., Cheng, H., Zhang, X., Zhai, M., Liu, C., Liang, L., Zhang, G., Luo, B., Tao, J., Liu, J., Zhao, H., Ren, S., Zhou, G., Liu, P., Xu, X., and Sun, Y.: Efficient Nitrate Formation in Fog Events Implicates Fog Interstitial Aerosols as Significant Drivers of Atmospheric Chemistry, Environmental Science & Technology. 58, 22298-22311, https://doi.org/10.1021/acs.est.4c09078, 2024.
Xu, Z., Wang, T., Wu, J., Xue, L., Chan, J., Zha, Q., Zhou, S., Louie, P. K. K., and Luk, C. W. Y.: Nitrous acid (HONO) in a polluted subtropical atmosphere: Seasonal variability, direct vehicle emissions and heterogeneous production at ground surface, Atmospheric Environment. 106, 100-109, https://doi.org/10.1016/j.atmosenv.2015.01.061, 2015.
Xuan, H., Liu, C., Zhang, P., Chu, B., Liang, L., Ma, Q., and He, H.: A Review of Laboratory Studies on the Heterogeneous Chemistry of NO_2: Mechanisms and Uptake Kinetics, The Journal of Physical Chemistry A. 129, 815-835, https://doi.org/10.1021/acs.jpca.4c07943, 2025.
Xuan, H., Zhao, Y., Ma, Q., Chen, T., Liu, J., Wang, Y., Liu, C., Wang, Y., Liu, Y., Mu, Y., and He, H.: Formation mechanisms and atmospheric implications of summertime nitrous acid (HONO)

during clean, ozone pollution and double high-level $PM_{2.5}$ and O_3 pollution periods in Beijing, Science of The Total Environment. 857, 159538, https://doi.org/10.1016/j.scitotenv.2022.159538, 2023.

Xuan, H., Liu, J., Zhao, Y., Cao, Q., Chen, T., Wang, Y., Liu, Z., Sun, X., Li, H., Zhang, P., Chu, B., Ma, Q., and He, H.: Relative humidity driven nocturnal HONO formation mechanism in autumn haze events of Beijing, npj Climate and Atmospheric Science. 7, 193, https://doi.org/10.1038/s41612-024-00745-8, 2024.

Yang, C., Dong, H., Chen, Y., Wang, Y., Fan, X., Tham, Y. J., Chen, G., Xu, L., Lin, Z., Li, M., Hong, Y., and Chen, J.: Machine Learning Reveals the Parameters Affecting the Gaseous Sulfuric Acid Distribution in a Coastal City: Model Construction and Interpretation, Environmental Science & Technology Letters. 10, 1045-1051, https://doi.org/10.1021/acs.estlett.3c00170, 2023.

Yang, C., Dong, H., Chen, Y., Xu, L., Chen, G., Fan, X., Wang, Y., Tham, Y. J., Lin, Z., Li, M., Hong, Y., and Chen, J.: New Insights on the Formation of Nucleation Mode Particles in a Coastal City Based on a Machine Learning Approach, Environmental Science & Technology. 58, 1187-1198, https://doi.org/10.1021/acs.est.3c07042, 2024.

Yang, J., Shen, H., Guo, M.-Z., Zhao, M., Jiang, Y., Chen, T., Liu, Y., Li, H., Zhu, Y., Meng, H., Wang, W., and Xue, L.: Strong marine-derived nitrous acid (HONO) production observed in the coastal atmosphere of northern China, Atmospheric Environment. 244, 117948, https://doi.org/10.1016/j.atmosenv.2020.117948, 2021.

Ye, C., Zhang, N., Gao, H., and Zhou, X.: Photolysis of Particulate Nitrate as a Source of HONO and NOx, Environmental Science & Technology. 51, 6849-6856, https://doi.org/10.1021/acs.est.7b00387, 2017.

Zha, Q., Xue, L., Wang, T., Xu, Z., Yeung, C., Louie, P. K. K., and Luk, C. W. Y.: Large conversion rates of NO_2 to HNO_2 observed in air masses from the South China Sea: Evidence of strong production at sea surface?, Geophysical Research Letters. 41, 7710-7715, https://doi.org/10.1002/2014GL061429, 2014.

Zhang, R., Minamikawa, R., Gen, M., Singh, N., Daniel, D., Li, Y. J., Wang, X., and Chan, C. K.: Evidence on Interfacial Reaction Governing NO_2 Hydrolysis in Deliquesced Aerosol Particles, Environmental Science & Technology. 59, 11708-11719, https://doi.org/10.1021/acs.est.5c05223, 2025a.

Zhang, W., Tong, S., Jia, C., Wang, L., Liu, B., Tang, G., Ji, D., Hu, B., Liu, Z., Li, W., Wang, Z., Liu, Y., Wang, Y., and Ge, M.: Different HONO Sources for Three Layers at the Urban Area of Beijing, Environmental Science & Technology. 54, 12870-12880, https://doi.org/10.1021/acs.est.0c02146, 2020.

Zhang, X., Tong, S., Jia, C., Zhang, W., Wang, Z., Tang, G., Hu, B., Liu, Z., Wang, L., Zhao, P., Pan, Y., and Ge, M.: Elucidating HONO formation mechanism and its essential contribution to OH during haze events, npj Climate and Atmospheric Science. 6, 55, https://doi.org/10.1038/s41612-023-00371-w, 2023.

Zhang, X., Tong, S., Jia, C., Zhang, W., Li, J., Wang, W., Sun, Y., Wang, X., Wang, L., Ji, D., Wang, L., Zhao, P., Tang, G., Xin, J., Li, A., and Ge, M.: The Levels and Sources of Nitrous Acid (HONO) in Winter of Beijing and Sanmenxia, Journal of Geophysical Research: Atmospheres. 127, e2021JD036278, https://doi.org/10.1029/2021JD036278, 2022.

Zhang, Y., Zheng, F., Feng, Z., Lian, C., Wang, W., Fan, X., Ma, W., Lin, Z., Li, C., Zhang, G., Yan, C., Zhang, Y., Kerminen, V. M., Bianch, F., Petäjä, T., Kangasluoma, J., Kulmala, M., and Liu, Y.:

Concentration and source changes of nitrous acid (HONO) during the COVID-19 lockdown in Beijing, Atmos. Chem. Phys., 24, 8569-8587, https://doi.org/10.5194/acp-24-8569-2024, 2024.

Zhang, Y., Liu, Y., Ma, W., Hua, C., Zheng, F., Lian, C., Wang, W., Xia, M., Zhao, Z., Li, J., Xie, J., Wang, Z., Wang, Y., Chen, X., Zhang, Y., Feng, Z., Yan, C., Chu, B., Du, W., Kerminen, V.-M., Bianchi, F., Petäjä, T., Worsnop, D., and Kulmala, M.: Changing aerosol chemistry is redefining HONO sources, Nature Communications. 16, 5238, https://doi.org/10.1038/s41467-025-60614-7, 2025b.

Zheng, J., Shi, X., Ma, Y., Ren, X., Jabbour, H., Diao, Y., Wang, W., Ge, Y., Zhang, Y., and Zhu, W.: Contribution of nitrous acid to the atmospheric oxidation capacity in an industrial zone in the Yangtze River Delta region of China, Atmos. Chem. Phys., 20, 5457-5475, https://doi.org/10.5194/acp-20-5457-2020, 2020.

Zhou, X., Zhang, N., TerAvest, M., Tang, D., Hou, J., Bertman, S., Alaghmand, M., Shepson, P. B., Carroll, M. A., Griffith, S., Dusanter, S., and Stevens, P. S.: Nitric acid photolysis on forest canopy surface as a source for tropospheric nitrous acid, Nature Geoscience. 4, 440-443, https://doi.org/10.1038/ngeo1164, 2011.